Inorg. Chem. **2009**, *48*, 4400−4410

Characterization of Intermediary Redox States of the Water Oxidation Catalyst, $[Ru(bpy)_2(OH_2)]_2O^{4+}$

Jonathan L. Cape,[†] Sergei V. Lymar,[‡] Travis Lightbody,[†] and James K. Hurst*,[†]

Department of Chemistry, Washington State University, Pullman, Washington 99164-4630, and Chemistry Department, Brookhaven National Laboratory, Upton, New York 11973-5000

Received January 20, 2009

Higher oxidation states of the μ-oxo bridged ruthenium "blue dimer" ($[Ru(bpy)_2(OH_2)]_2O^{4+}$) have been characterized by redox titration measurements, resonance Raman (RR) spectroscopy, EPR spectrometry, and pulse radiolysis. The cumulative results indicate that the progression of accessible oxidation states in acidic media is **{3,3}** → **{3,4}** → **{4,4}** → **{5,5}**, but changes to **{3,3}** → **{3,4}** → **{4,5}** → **{5,5}** above pH 2. Although the reaction $2\{4,5\} + 2H_2O \rightarrow 2\{3,4\} + O_2$ is thermodynamically favorable, no O_2 was detected during the decay of **{4,5}** to **{3,4}**. One-electron oxidation of **{3,4}** by radiolytically generated sulfate and carbonate radicals allowed determination of the **{4,4}** optical spectrum in neutral and alkaline media, where it exists only as a short-lived transient species. This spectrum was identical to that previously reported for **{4,4}** in acidic media; this observation and comparative RR spectra suggest that its molecular formula is $[Ru(bpy)_2(OH)]_2O^{4+}$, that is, both Ru atoms contain a coordinated hydroxo ligand. Upon application of an acidic pH jump, electrochemically prepared **{4,5}** underwent disproportionation to **{4,4}** and **{5,5}**, as determined from changes in the EPR spectra of the solutions. These studies clarify the nature of redox transients formed during water oxidation catalysis by the "blue dimer", thereby providing information that is critical to performing accurate mechanistic analyses.

Introduction

Development of complex ions that can function as effective and robust catalysts for water oxidation is a long-sought goal of coordination chemists[1] that is receiving renewed attention[2] in light of rising global demands for energy derived from alternative sources and effective atmospheric pollution abatement methodologies. By providing insights into the critical factors controlling reactivity, mechanistic studies on existing homogeneous catalysts can be expected to play an important role in the evolution of superior catalysts suitable for technological applications. The most extensively studied of the known catalysts is the ruthenium "blue dimer", i.e., $[Ru(bpy)_2(OH_2)]_2O^{4+}$ (hereafter denoted **{3,3}**),[3] whose water oxidizing properties were initially recognized by Meyer and co-workers[3] in the mid-1980s and which has been extensively studied in several laboratories since then.[4−6] Although a consensus mechanism has not yet been reached, it is clear from this body of work that the catalyzed water oxidation reaction is complex and involves numerous elementary reaction steps and intermediary oxidation states. There is general agreement that the O_2-evolving species is reached upon oxidation to **{5,5}**, a reaction constituting net $4e^-$ oxidation of **{3,3}** that is accompanied by deprotonation of the coordinated aquo ligands. However, the identities of some of the accumulating intermediary oxidation states and other reaction transients detected during chemical and photochemical oxidations are less certain. Compounding the problem is a current absence of structural information on key reaction intermediates, e.g., a presumed peroxo-bound intermediate which, alternatively, has been suggested to form by coupling of water to a ruthenyl oxo atom in **{5,5}**[5,6] or water addition

* To whom correspondence should be addressed. E-mail: hurst@wsu.edu. Tel: 509-335-7848. Fax: 509-335-8867.
† Washington State University.
‡ Brookhaven National Laboratory.

(1) Creutz, C.; Sutin, N. *Proc. Natl. Acad. Sci., U.S.A.* **1975**, *72*, 2858–2862.
(2) Eisenberg, R.; Gray, H. B. *Inorg. Chem.* **2008**, *47*, 1697–1699, and subsequent "Making Oxygen" Forum papers.
(3) Gilbert, J. A.; Eggleston, D. A.; Murphy, W. A., Jr.; Geselowitz, D. A.; Gersten, S. W.; Hodgson, D. J.; Meyer, T. J. *J. Am. Chem. Soc.* **1985**, *107*, 3855–3864.
(4) Leading references to the literature can be found in refs 5 and 6.
(5) Liu, F.; Concepcion, J. J.; Jurss, J. W.; Cardolaccia, T.; Templeton, J. L.; Meyer, T. J. *Inorg. Chem.* **2008**, *47*, 1727–1752.
(6) Hurst, J. K.; Cape, J. L.; Clark, A. E.; Das, S.; Qin, C. *Inorg. Chem.* **2008**, *47*, 1753–1764.

10.1021/ic9001219 CCC: $40.75
Published on Web 04/16/2009

via bipyridine ligand radical intermediates to form a coordinated endoperoxide.[6] Continued advances in our understanding of this reaction are critically dependent upon accurate characterization of the species present under differing reaction conditions. For example, understanding mechanisms of "blue" dimer-catalyzed photosensitized oxidation of water[7] requires accurate assessment of the extent to which **{5,5}** accumulates under steady-state conditions imposed by continuous photolysis. This assessment, in turn, depends critically upon knowledge of the thermodynamic properties and physical characteristics of the accumulating intermediary redox states of the catalyst, which are generally the dominant species in solution.[8] Furthermore, several theoretical investigations of this reaction have recently been initiated to address aspects that are not amenable to direct experimentation.[6,9−11] Evaluation of the accuracy of these models rests upon their ability to predict experimentally measurable properties of the various accessible oxidation states.

We report herein results from various studies that provide an extensive characterization of the physical properties of the **{4,4}** and **{4,5}** ions, including structures, thermodynamics, and reaction dynamics; emphasis is placed upon their properties in neutral media (pH 5−9), because published work has dealt primarily with these properties in strongly acidic solutions.[5,6]

Experimental Section

Chemicals. The ligand 4,4′-dicarboxyethyl-2,2′bipyridine (dcb) was prepared by addition of absolute ethanol to the acid chloride of 4,4′-dicarboxy-2,2′-bipyridine.[12] The complex ions, $Ru(bpy)_3^{2+}$, $Ru(dcb)_2bpy^{2+}$, and $[Ru(bpy)_2(OH_2)]_2O^{4+}$, were prepared by standard procedures[3,13−17] and isolated as their perchlorate salts. The purity of the μ-oxo dimer was verified spectrophotometrically by titrating **{3,3}** to **{3,4}** with Ce(IV) to confirm the presence of isosbestic points at 510, 380, and 310 nm.[17] The $[Os(bpy)_2(OH_2)]_2O^{4+}$ ion was synthesized from $Os(bpy)_2CO_3$ essentially as described in the literature,[18,19] except that 0.1 M $HClO_4$ was used as supporting electrolyte during the final electrolysis step. $H_2{}^{18}O$-enriched $[Ru(bpy)_2(OH_2)]_2O^{4+}$ was prepared by incubating natural abundance **{3,3}** in 95% $H_2{}^{18}O$ (Cambridge Isotope Laboratories) for 3 h at 23 °C, after which oxidation to **{3,4}** with 2 mM potassium persulfate ($K_2S_2O_8$)[20] effectively quenched further exchange.[21] Because $[Os(bpy)_2(OH_2)]_2O^{4+}$ underwent water exchange at a considerably slower rate than the Ru analog, and also slowly underwent "spontaneous" oxidation in solution to the **{3,4}** state, the corresponding water exchange reaction was carried out in an electrochemical cell that allowed maintenance of its **{3,3}** state over the time interval required to reach equilibrium at the cis-aqua positions. The cell constructed for this purpose was a 0.2 cm path length optical cell fitted with Pt gauze working and auxiliary electrodes, a design which both minimized the amount of $H_2{}^{18}O$ required for the study and allowed convenient optical and resonance Raman (RR) spectroscopic characterization of the electrolyzed solution. Typically, the cell containing 0.6 mL of ∼500 μM Os dimer in 95% $^{18}OH_2$ was poised at −0.2 V vs Ag/AgCl at room temperature for two hours, during which time the solution was periodically agitated to promote convection to the electrode surface. Complexes containing 1:1 $^{18}O/^{16}O$ in their cis-aqua positions were similarly prepared by these respective methods from **{3,3}** ions incubated in 50% $H_2{}^{18}O$. Other reagents were best-available grades from commercial suppliers and were used without further purification. All solutions were prepared in reverse osmosis-deionized purified water.

Electrochemical Methods. Cyclic voltammetry was performed on a BAS 1200 electrochemical analyzer using a glassy carbon working electrode, Pt auxiliary electrode, and an Ag/AgCl reference electrode in a water jacketed cell. The reference electrode was isolated with a second salt bridge from the working electrode compartment to prevent Cl^- contamination of analyte solutions. Two methods were used in performing constant potential electrolysis (CPE) redox titrations and redox poising experiments involving $[Ru(bpy)_2(OH_2)]_2O^{4+}$. The first technique employed a carbon fiber flow electrode, as previously described by Yamada et al.[17] The second technique, which was more amenable to temperature dependent studies, employed a standard two-compartment CPE cell using Pt gauze electrodes containing a fritted glass divider to separate the working and auxiliary electrode compartments. Temperature was controlled by immersing the electrolysis cell in a water bath. An isolated $Hg/HgSO_4$ reference electrode was used in these experiments. Chemical redox titrations at neutral pH were performed using a slightly modified version of a previously described procedure, which relies upon quantitative oxidation of $Os(bpy)_3^{2+}$ to $Os(bpy)_3^{3+}$.[17] Briefly, 40 μM solutions of **{3,3}** in 50 mM potassium triflate and 10 mM phosphate, pH 7.0, were redox-poised at the desired potential in the temperature controlled CPE cell. When the current dropped to a constant value, 500 μL portions were added to 500 μL of 150−300 μM $Os(bpy)_3^{2+}$ in 0.5 M triflic acid to give a final solution whose pH was ∼0.3; under these experimental conditions, $Os(bpy)_3^{2+}$ quantitatively reduces the higher oxidation states of the ruthenium μ-oxo dimer to **{3,3}**, forming $Os(bpy)_3^{3+}$. The extent of oxidation was determined spectrophotometrically by using an $Os(bpy)_3^{2+/3+}$ difference extinction coefficient of $\Delta\varepsilon_{480} = 1.38 \times 10^4\ M^{-1}\ cm^{-1}$ and correcting the spectra for absorption by **{3,3}**.[17]

Spectrometric Methods. RR spectra were acquired by focusing backscattered light from the sample onto the entrance slit of an Acton Spectro-Pro 2300i single monochromator, from which signal intensities were measured using a Roper Scientific Spec 10:256E

(7) Rotzinger, F. P.; Munavalli, S.; Comte, P.; Hurst, J. K.; Grätzel, M.; Pern, F.-J.; Frank, A. J. *J. Am. Chem. Soc.* **1987**, *109*, 6619–6626.
(8) Cape, J. L.; Hurst, J. K. *J. Am. Chem. Soc.* **2008**, *130*, 827–829.
(9) Yang, X.; Baik, M.-H. *J. Am. Chem. Soc.* **2004**, *126*, 13222–13223.
(10) Yang, X.; Baik, M.-H. *J. Am. Chem. Soc.* **2006**, *128*, 7476–7485.
(11) Batista, E. R.; Martin, R. L. *J. Am. Chem. Soc.* **2007**, *129*, 7224–7225.
(12) Garelli, N.; Vierling, P. *J. Org. Chem.* **1992**, *57*, 3046–3051.
(13) Sullivan, B. P.; Salmon, D. J.; Meyer, T. J. *Inorg. Chem.* **1978**, *17*, 3334–3341.
(14) Damrauer, N. H.; Boussie, T. R.; Devenney, M.; McCusker, J. K. *J. Am. Chem. Soc.* **1997**, *119*, 8253–8268.
(15) Anderson, P. A.; Anderson, R. F.; Furue, M.; Junk, P. C.; Keene, F. R.; Patterson, B. T.; Yeomans, B. D. *Inorg. Chem.* **2000**, *39*, 2721–2728.
(16) Elliott, M. C.; Hershenhart, E. J. *J. Am. Chem. Soc.* **1982**, *104*, 7519–7526.
(17) Yamada, H.; Hurst, J. K. *J. Am. Chem. Soc.* **2000**, *122*, 5303–5311.
(18) Gilbert, J. A.; Geselowitz, D. A.; Meyer, T. J. *J. Am. Chem. Soc.* **1986**, *108*, 1493–1501.
(19) Madhiri, N.; Finklea, H. O. *Langmuir* **2006**, *22*, 10643–10651.
(20) Comte, P.; Nazeruddin, M. K.; Rotzinger, F. P.; Frank, A. J.; Grätzel, M. *J. Mol. Catal.* **1989**, *52*, 63–84.
(21) Yamada, H.; Koike, T.; Hurst, J. K. *J. Am. Chem. Soc.* **2001**, *123*, 12775–12780.

thermoelectrically cooled CCD.[22] The 496.5 nm line of a Coherent Innova 400 Ar ion laser operated at 100 mW power was used as light source; the backscattered light was passed through a Kaiser Optical holographic notch filter to remove the elastically scattered component prior to entering the spectrophotometer. Typical spectra involved coadding a series of no more than twenty 10 s exposures. No sample degradation was detected under these conditions, as determined by both RR and optical spectroscopy. Samples in which either intermediate or **{5,5}** redox states of the Ru dimer were generated photochemically used the probe laser itself as the light source.[8] These samples contained 10−60 μM of either $Ru(bpy)_3^{2+}$ ($E^o(Ru^{II/III}) = 1.27$ V(NHE)) or $Ru(dcb)_2bpy^{2+}$ ($E^o(Ru^{II/III}) = 1.51$ V(NHE)) as photosensitizers to generate the desired redox states, 5 mM potassium persulfate as electron acceptor and (typically) 100 μM **{3,3}**. Under these experimental conditions, the steady-state concentration levels of the various redox states of the dimer could be manipulated by varying the photosensitizer identity and concentration, allowing us to probe either intermediate or **{5,5}** redox states as majority species in solution. RR spectra of the Os dimer were obtained in the electrochemical cell described above by oxidizing the solvent-equilibrated **{3,3}**/**{3,4}** mixture to **{4,5}** by constant potential electrolysis (CPE) at 0.8 V vs Ag/AgCl for an hour. Following removal of the electrodes, resonance Raman (RR) spectra of the samples were immediately obtained in situ. Unlike the more strongly oxidizing ruthenium analog, the osmium **{4,5}** ion is stable for the duration of these measurents.[23] RR band energies were determined by measuring their displacement from the bipyridine ν_{15} ring breathing mode,[24] which is at 1042 cm^{-1} in the ruthenium **{3,4}** ion and 1046 cm^{-1} in the osmium **{3,4}** ion.[25]

EPR spectra were obtained using a Bruker 300e EPR spectrometer equipped with a liquid nitrogen dewar insert for measurements at 77 K. Optical spectra were recorded on an HP 8452A diode array spectrophotometer.

Pulse Radiolysis. Sample solutions were buffered at pH 7.1−7.2, pH 9.2, or pH 10.5 with 2−7 mM phosphate, 2 mM borate, or 30 mM carbonate, respectively, and contained 0−50 μM ruthenium dimer in its **{3,4}** oxidation state. The latter was prepared by incubating **{3,3}** with 0.1−2 mM persulfate ($S_2O_8^{2-}$) for several minutes. This reaction exhibited approximate second-order kinetics, for which a rate constant of $k_{second} = 14 \pm 1\ M^{-1}\ s^{-1}$ was determined at 23 °C in 50 mM phosphate, pH 7.0. Under these conditions, oxidation to **{3,4}** was stoichiometric, as determined spectrophotometrically; these solutions, containing slight excess of $S_2O_8^{2-}$, were stable for at least 24 h. All solutions were thoroughly purged with either argon or nitrous oxide prior to pulse radiolysis, which was carried out with 2 MeV electrons from a Van de Graaff accelerator; pulse widths were between 0.06 and 0.3 μs, with most data taken using a 0.1 μs pulse. Solutions were contained in a quartz cell that had a 2 cm optical path length. In most cases, samples were discarded after being subjected to a single radiation pulse. For kinetics recorded on a time scale of less than 100 μs, the analyzing Xe arc light source was pulsed.

For quantitative analysis, the radiation yields of radicals (in number of radicals per 100 eV absorbed energy) were taken as $G(SO_4^{\bullet -}) = G(e_{aq}^-) = 2.8$ and $G(H^\bullet) = 0.6$. Radiation dosimetry was performed with N_2O-saturated 10 mM KSCN solutions using $G\varepsilon = 4.87 \times 10^4$ ions $(100\ eV)^{-1}\ M^{-1}\ cm^{-1}$ for the $(SCN)_2^{\bullet -}$ radical at 472 nm. The radiation dose was recorded for each kinetic run, which allows accurate determination of concentrations of all radicals produced. All experiments were done at 21−23 °C. Kinetic modeling was carried out with the INTKIN software developed at the Brookhaven National Laboratory by H. A. Schwarz.[26]

Results and Discussion

Electrochemical Properties. The electrochemical response of **{3,3}** was extensively studied by Meyer and coworkers in their original paper describing the catalytic activity of this ion toward water oxidation.[3] Above pH ∼2, cyclic and differential pulse voltammograms showed two to three redox transitions when swept to positive potentials, indicating formation of two stable higher oxidation states. Although the wave appearing at the highest potential was ill-defined and nonstoichiometric, the first two waves exhibited relative amplitudes of ∼1:2 and CPE coulometric measurements indicated that oxidation of **{3,4}** required two electrons,[27] supporting their assignment of the following oxidation sequence: **{3,3}** → **{3,4}** → **{4,5}** → **{5.5}**, with the **{4,4}** state presumably being unstable with respect to disproportionation. Below pH ∼2, the two waves corresponding to the higher oxidations coalesced, giving rise to an apparent 3-electron oxidation, i.e., the sequence **{3,3}** → **{3,4}** → **{5.5}**. Using a rapid CPE technique to prepare samples at various redox poises, we subsequently confirmed by direct redox titration with $Os(bpy)_3^{2+}$ that the highest oxidation state achieved in acidic solution was indeed **{5,5}**.[17] The redox titration curve obtained was non-Nernstian, and could be adequately fitted only by assuming that the higher oxidation process involved two redox steps whose potentials differed by less than 60 mV; voltammetric methods are not sufficiently sensitive to resolve these steps under the experimental constraints imposed by the system.

We have now extended these redox titration measurements to neutral solutions. Typical results are presented in Figure 1, where a conventional CPE cell has been used to set the redox poise of the solutions.[28] As predicted by the CV data, at pH 7.2, a one-electron oxidation occurs at ∼0.60 V vs NHE, which is followed by a temperature-dependent second oxidative step at ∼1.1 V showing variable stoichiometry. The slopes of these curves exhibited non-Nernstian behavior with n values less than unity. Apparent stoichiometries for the second oxidation step determined from the curves are ∼2.1, ∼1.4, and ∼1.2 equivalents above **{3,3}** at 4, 23, and 50 °C, respectively. At this pH, solvent breakdown prevents oxidation of the complex to **{5,5}**.[3] The highest attainable

(22) Pollard, J. A.; Zhang, D.; Downing, J. A.; Knorr, F. J.; McHale, J. L. *J. Phys. Chem. A* **2005**, *109*, 11443–11452.

(23) This Os **{4,5}** ion has been reported to undergo decomposition to **{3,4}** within a few minutes at pH 8, and more rapidly in strongly alkaline media, presumably by oxidative degradation of the bipyridine ligands (see ref 18). At pH 7, however, we found that the electrochemically generated Os **{4,5}** ion was stable for several hours, as determined spectrophotometrically.

(24) Strommen, D. P.; Mallick, P. K.; Danzer, G. D.; Lumpkin, R. S.; Kincaid, J. R. *J. Phys. Chem.* **1990**, *94*, 1357–1366.

(25) Schoonover, J. R.; Ni, J. F.; Roecker, L.; White, P. S.; Meyer, T. J. *Inorg. Chem.* **1996**, *35*, 5885–5892.

(26) The numerical integration method used in this program is the following package: Brown, P. N.; Hindmarsh, A. C.; Byrne, G. D. *DVODE*; Lawrence Livermore National Laboratory and Exxon Research and Engineering Co.: Livermore, CA, and Paulsboro, NJ.

(27) Raven, S. J.; Meyer, T. J. *Inorg. Chem.* **1988**, *27*, 4478–4483.

(28) The high surface/volume carbon flow-through electrode used for rapid CPE in acidic solutions (see ref 17) is ineffective at pH >2 because interfering direct electrolysis of H_2O becomes excessive.

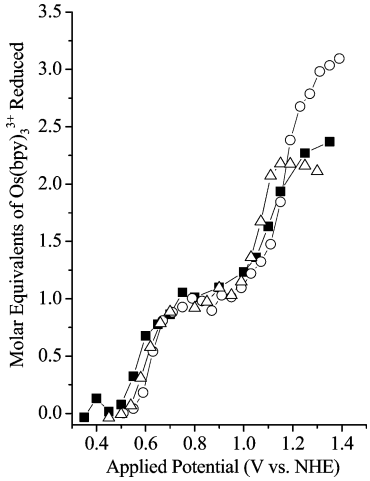

Figure 1. Oxidizing equivalents measured in electrolyzed solutions of the μ-oxo ruthenium dimer. In these measurements, 40 μM **{3,3}** in 10 mM phosphate, pH 7.2, was first oxidized by CPE and then reacted with an equal volume of 300 μM $Os(bpy)_3^{2+}$ in 0.5 M triflic acid. The acidification that accompanied mixing with $Os(bpy)_3^{2+}$ ensured that the dimer quantitatively regenerated **{3,3}** with formation of an equivalent amount of $Os(bpy)_3^{3+}$.[17] Electrolyses were performed at 4° (open circles), 23° (closed squares), and 50°C (open triangles).

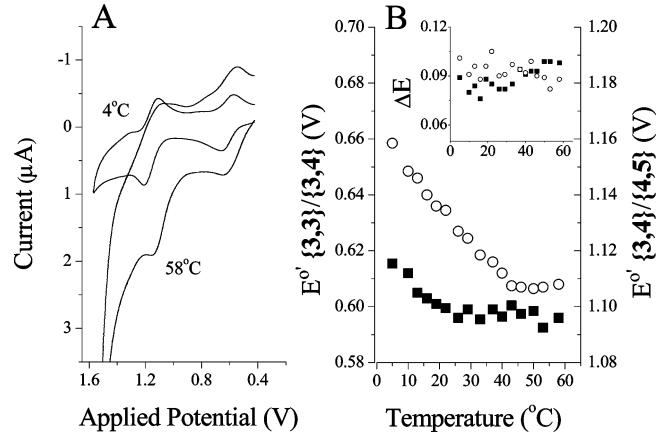

Figure 2. Cyclic voltammetric response of $[Ru(bpy)_2(OH_2)]_2O^{4+}$. Cyclic voltammetry was performed as described in the Experimental Section on 0.5 mM **{3,3}** in 100 mM potassium triflate, 5 mM phosphate, pH 7.2. (A) Representative cyclic voltammograms at 4 and 58 °C (100 mV/s sweep rate). (B) Temperature dependence of $E_{1/2}$ values for the first (closed squares, left axis) and second (open circles, right axis) oxidation waves shown in panel A. Inset: temperature dependence of anodic and cathodic peak-to-peak separations of redox waves shown in panels A and B. All potentials are given versus NHE.

oxidation state under these experimental conditions is therefore the intermediary one in the overall reaction sequence. Meyer and co-workers have reported that the **{4,5}** ion is relatively stable at 5 °C, but slowly decomposes at higher temperatures.[29] We have observed a similar autoreduction of the CPE-generated intermediate in this study (described below), which gives **{3,4}** as the final product. Given the nature of this instability, the redox titration data presented above can be interpreted as indicating that the second redox step is a two-electron oxidation of **{3,4}** to **{4,5}**, and that the inability to achieve the correct stoichiometry at higher temperatures is a consequence of competing electrochemical formation and spontaneous decay of **{4,5}** on the relatively long time scale required for redox equilibration by conventional CPE methods.

These conclusions are also supported by cyclic voltammetric (CV) measurements, where two quasi-reversible oxidation waves are observed that exhibit temperature-invariant relative amplitudes of ~1:1.5 (Figure 2A). Also evident in the voltammograms is the onset of breakdown of the aqueous solvent, which appears at potentials ~300 mV more positive than that of the second wave. The temperature-dependence of the midpoint potentials ($E^{o'}$) is summarized in Figure 2B, as are the ΔE ($E_{pa} - E_{pc}$) values, which provide a qualitative index of the relative reversibility of these reactions. The insensitivity of ΔE and the ratios of the peak-to-peak currents for the two oxidation steps to temperature, as well as the approximately equal currents observed for anodic and cathodic half-waves for each step (Figure 2A), indicate that decomposition of **{4,5}** is insignificant at all temperatures on the CV time scale (<1 min).

Characterization of {4,5}. Resonance Raman Spectra. The resonance-enhanced Raman spectra of these ions exhibit three readily detectable ^{18}O-isotope sensitive bands, assignable as the Ru−O−Ru symmetric stretching frequency (ν_{sym}(Ru−O−Ru)), its first overtone ($2 \times \nu_{sym}$), and when the ruthenyl group is present, the Ru═O stretching vibrational band ($\nu_{Ru=O}$).[17,21,30,31] The ν_{sym}(Ru−O−Ru) band appears at 360−400 cm^{-1}, and is only weakly dependent upon the oxidation state of the dimer. However, its scattering intensity is much less in the higher oxidation states; correspondingly, in redox titrations, its intensity decreases dramatically with progressive oxidation of the complex. Substitution of ^{18}O in the bridging position causes ν_{sym}(Ru−O−Ru) for a given oxidation state to decrease by $\Delta\nu = 2-8$ cm^{-1}, consistent with the nearly linear geometry of the Ru−O−Ru bridge. In acidic media, the only accessible oxidation state exhibiting the Ru═O mode is **{5,5}**, which shifts from 818 cm^{-1} to 780 cm^{-1} ($\Delta\nu = 38$ cm^{-1}) upon substitution of ^{18}O in the terminal aqua positions. Although the Ru═O band appears in the same spectral region as the O−O stretching mode of peroxides, these can be distinguished by measuring the spectra of mixed isotopomers. Specifically, when the $^{18}O/^{16}O$ ratio is 1/1, the Ru═O modes exhibit two bands corresponding to the individual Ru═^{16}O and Ru═^{18}O isotopomer stretches, whereas the O−O stretching mode exhibits three bands in a 1:2:1 intensity pattern, corresponding to the statistically distributed $^{16}O-^{16}O$, $^{18}O-^{16}O$, and $^{18}O-^{18}O$ isotopomers.

Based upon the pH dependence of CV-derived $E_{1/2}$ values published by the Meyer group,[3] the coordinated cis-aqua ligands of **{3,3}** should be completely deprotonated to ruthenyl oxo atoms upon oxidation to **{4,5}** in neutral solutions, i.e., possessing the structure $[Ru(bpy)_2(O)]_2O^{3+}$. Results of a redox titration with RR detection using CPE to titrate through the **{3,4}/{4,5}** couple are shown in Figure 3; this experiment was performed at 4 °C to minimize **{4,5}** decomposition. As expected, the **{3,4}** ν_{sym}(Ru−O−Ru) band

(29) Binstead, R. A.; Chronister, C. W.; Ni, J.; Hartshorn, C. M.; Meyer, T. J. *J. Am. Chem. Soc.* **2000**, *122*, 8464–8473.

(30) Hurst, J. K.; Zhou, J.; Lei, Y. *Inorg. Chem.* **1992**, *31*, 1010–1017.
(31) Lei, Y.; Hurst, J. K. *Inorg. Chem.* **1994**, *33*, 4460–4467.

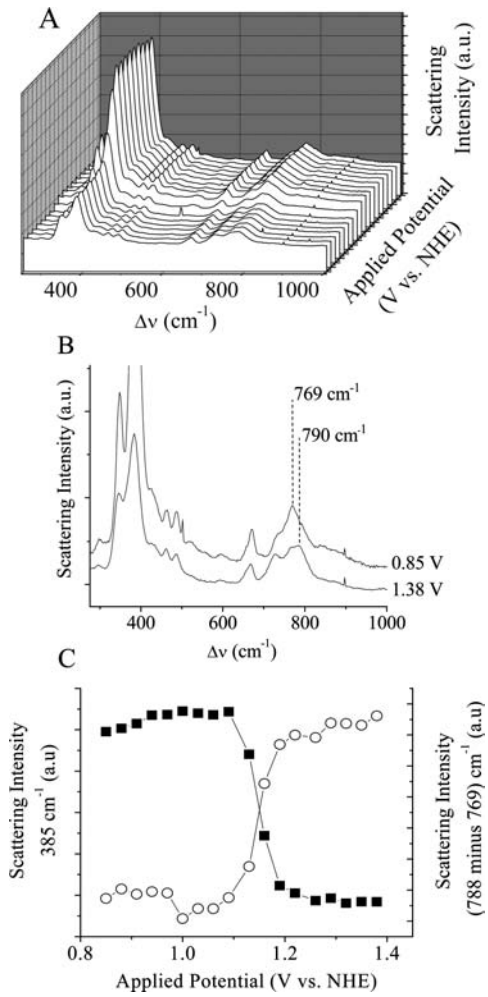

Figure 3. Resonance Raman spectra of CPE-oxidized **{3,4}**. Conditions: 300 μM **{3,4}**, 100 mM phosphate, pH 7.2, electrolyzed at 4 °C. (A) Spectroelectrochemical titration from 0.85 to 1.38 V. (B) End point spectra of the dimer poised at 0.85 V (**{3,4}**), and at 1.38 V vs NHE (**{4,5}**) (C) Resonance Raman peak intensities as a function of applied potential for **{3,4}** ν_{sym}(Ru−O−Ru) (385 cm^{-1}, closed squares) and **{4,5}** ν(Ru═O) (790 cm^{-1}, open circles), plotted as the 790 cm^{-1} minus 769 cm^{-1} difference intensity.

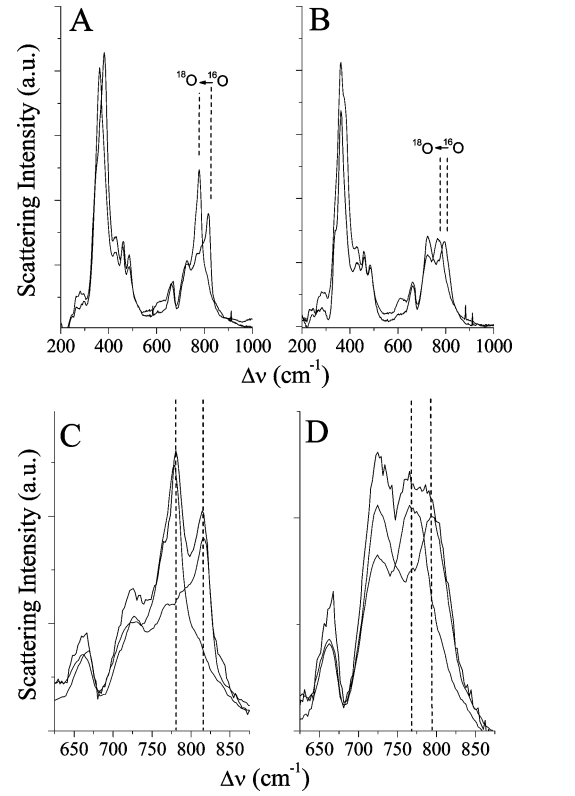

Figure 4. Resonance Raman comparison of the **{5,5}** and **{4,5}** redox states in 5 mM $K_2S_2O_8$, 0.1 M phosphate, pH 7.2, containing 10−60 μM photosensitizer. (A) Spectra of the $^{18}O/^{16}O$ isotopomers of **{5,5}** displaying a ∼37 cm^{-1} shift to lower energy of ν(Ru═O) at 818 cm^{-1} upon ^{18}O substitution.[17,21] The small shift in ν_{sym}(Ru−O−Ru) observed at ∼385 cm^{-1} is due to a small contribution from the **{3,4}** state in the spectrum of the ^{16}O-labeled dimer. (B) Spectra of the $^{18}O/^{16}O$ isotopomers of the **{4,5}** redox state displaying a ∼24 cm^{-1} shift of ν(Ru═O) at 796 cm^{-1} to lower energy upon ^{18}O substitution. C) Mixed isotope preparation of **{5,5}** as a 1:1 distribution of $^{18}O/^{16}O$ in the cis-aqua positions (black) with a comparison to the individual spectra of the ^{18}O-labeled and ^{16}O-labeled dimer species (gray). (D) Mixed isotope preparation of **{4,5}** as a 1:1 distribution of $^{18}O/^{16}O$ in the cis-aqua positions (black) with a comparison to the individual spectra of the ^{18}O-labeled and ^{16}O-labeled dimer species (gray).

at 385 cm^{-1} and its first overtone at 769 cm^{-1} decreased in intensity as the titration progressed through the $E_{1/2}$ value of 1.15 V, accompanied by simultaneous appearance of a new band at ∼790 cm^{-1} (Figures 3B,C), provisionally attributable to the Ru═O stretching mode in **{4,5}**. It is apparent, however, that the procedures used did not allow for complete oxidation of **{3,4}** to **{4,5}**. This problem is undoubtedly a consequence of the instability of **{4,5}**; at room temperature, the contribution of **{3,4}** to the RR spectrum was too large to clearly resolve the 790 cm^{-1} band. However, application of a previously described photochemical method[8] permitted generation of **{4,5}** as the major species in solution. With this method, which involves photosensitized formation of $Ru(bpy)_3^{3+}$ ($E^o(Ru^{II/III})$ = 1.27 V(NHE)) as a chemical oxidant, oxidation of the dimer is considerably more rapid than by CPE, thereby increasing the steady-state concentration of **{4,5}**. Furthermore, by using a more strongly oxidizing analog as photosensitizer, in this case, $Ru(dcb)_2bpy^{3+}$ ($E^o(Ru^{II/III})$ = 1.51 V(NHE)),[8] it was possible to generate **{5,5}** as the majority species, thereby allowing direct comparison of the RR spectra of the two oxidized dimer states. Figure 4A shows spectra of photochemically generated **{5,5}**, exhibiting a band at 818 cm^{-1} that underwent a ∼37 cm^{-1} downfield shift to 781 cm^{-1} upon substituting $H_2{}^{18}O$ for $H_2{}^{16}O$ in the *cis*-aqua positions of the complex. Figure 4B shows the analogous ^{18}O labeling experiment for the photochemically generated **{4,5}**, where the 796 cm^{-1} band shifts to 772 cm^{-1} ($\Delta\nu$ = 24 cm^{-1}) to lower energies upon isotopic substitution in the cis-aqua positions. Panels C and D show the corresponding spectra obtained when **{3,3}** was incubated in $H_2{}^{16}O/H_2{}^{18}O$ to achieve a 1:1 $^{16}O/^{18}O$ isotope distribution in the cis-aqua positions. As expected, the mixed-isotope RR spectra of **{5,5}** exhibited only two bands corresponding to the frequencies of the Ru═O isotopomers, rather than a 1:2:1 three-band pattern indicative of bound peroxy species. Similarly, the spectra of **{4,5}** under these conditions gave a partially resolved doublet that fits well to an assumed contribution from each isotopomer, but clearly ruling out a bound peroxy group (which would require the presence of a third band at ∼784 cm^{-1} with twice the intensity of the two existing bands).[30] Resonance Raman spectra were also taken for the analogous

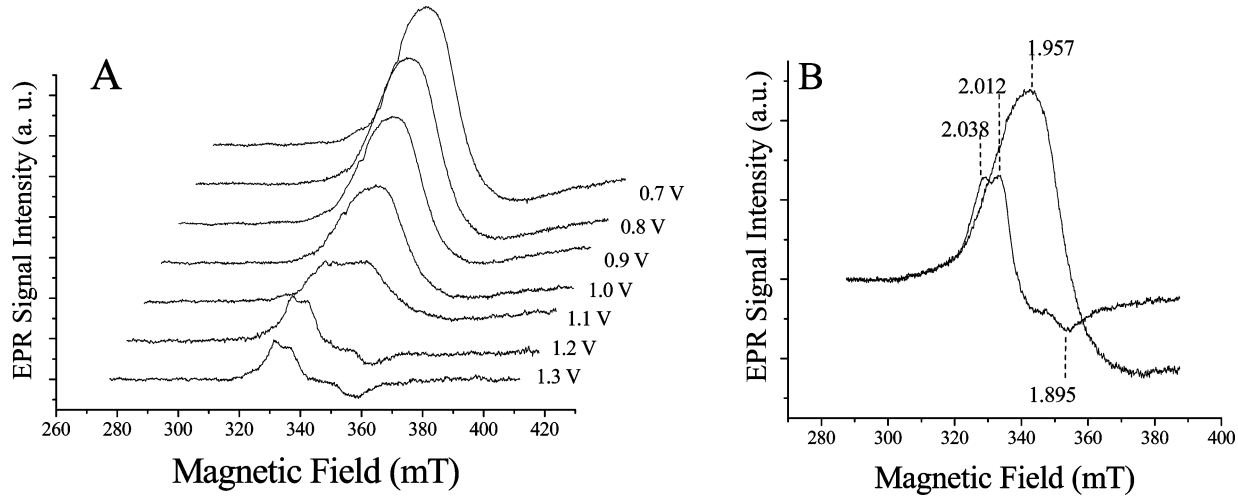

Figure 5. CW-EPR spectra of **{3,4}** and **{4,5}** at 77 K. (A) CPE titration in 100 mM phosphate, pH 7.2; (B) spectra at 0.7 and 1.3 V applied potentials. Instrument parameters: ~9.484 GHz microwave frequency, 100 kHz modulation frequency, 15 gauss modulation amplitude, 20 ms conversion time, 5 ms time constant, 20 mW microwave power.

osmium dimer, $[Os(bpy)_2(OH_2)]_2O^{4+}$, which is relatively stable in its **{4,5}** state,[23] to verify the Ru=O band assignments made for the ruthenium analog. In CPE electrochemical titrations, the **{4,5}** state of the Os dimer appeared with an apparent $E_{1/2} = 0.81$ V (NHE), similar to values obtained by CV analysis.[18] Major changes in the corresponding RR spectra were loss in intensity of the strong ν_{sym}(Os−O−Os) band associated with the **{3,4}** oxidation state, which was accompanied by the appearance of a band centered at 831 cm^{-1} that shifted to 812 cm^{-1} ($\Delta\nu = 19$ cm^{-1}) upon substitution of $H_2{}^{18}O$ in the cis-aqua positions (see Figure S1 in the Supporting Information). Thus, it is clear that a terminal M=O stretching mode is a dominant feature of the RR spectra of **{4,5}** in both complexes.

EPR Spectra. At 77 K, the paramagnetic μ-oxo ions exhibit broad rhombic signals in the $g \approx 2$ region (Figure 5), as expected for complexes that contain no symmetry axis greater than 2. The g-tensors in the spectrum observed for **{3,4}** are unresolved, and overall the spectrum is qualitatively similar to spectra previously reported for this ion at lower pH,[17,31] albeit with an apparent g-value that is shifted substantially downfield ($g = 1.957$ at pH 7 vs $g = 1.770$ at pH 1). These differences may be due to effects on spin−orbit coupling arising from partial deprotonation of the cis-aqua ligands in the more alkaline media, forming $[Ru(bpy)_2(OH)]_2O^{3+}$.[3] Figure 5A shows the transition from **{3,4}** to **{4,5}** by CPE redox titration that occurs under these conditions with an apparent $E_{1/2} = 1.15$ V, and Figure 5B shows the corresponding EPR spectra of the two oxidation states. These observations clearly establish the redox intermediate as **{4,5}**, because the alternative intermediary redox state, i.e., **{4,4}**, must be zero- or even-spin, and therefore should be EPR-silent in the X-band spectrum. Formation of **{4,5}** is associated with the appearance of a new rhombic signal with partially resolved g tensors ($g_x = 2.039$, $g_y = 1.995$, $g_z = 1.895$; $g_{avg} = 1.976$), consistent with assignment as an $S = 1/2$ spin state.[32] The intensity of this signal increased ~5-fold upon lowering the temperature from 77 to 15 K, and exhibited no indication of saturation at microwave powers as high as 100 mW, suggesting that the signal originates from an unpaired spin on the Ru−O−Ru core. Overall, these EPR spectra exhibit features that are similar to those reported for mixed-valence Ru_2 **{2,3}** complexes in which there is a moderate degree of delocalization across the bridging ligand.[33−35]

The presence of 50 mM potassium trifluoromethanesulfonate (triflate), which was used as supporting electrolyte in some of the titrations, resulted in a sharpening of the features of the **{3,4}** spectrum with an increase in its rhombicity ($g_x = 2.003$, $g_y = 1.934$, $g_z = 1.874$; $g_{avg} = 1.937$). Triflate anion at these concentration levels in room temperature solutions had no effect upon the catalytic O_2 evolution activity of the complex, however. One possible explanation is that triflate interacts with **{3,4}** in the cryogenic samples via H-bonding at the cis-aqua positions, resulting in a conformationally "frozen" state exhibiting enhanced anisotropy. Triflate also had no detectable influence upon the EPR signal of **{4,5}**, possibly because its ruthenyl centers are fully deprotonated and therefore possess no donors suitable for H-bonding to triflate.

Optical Spectra and Reaction Dynamics. At pH 7, CPE-generated **{4,5}** is characterized by a broad asymmetric visible absorption band ($\lambda_{max} = 492$ nm, $\varepsilon_{492} = 8.9 \times 10^3$ M^{-1} cm^{-1}) that extends well into the red part of the spectrum (see Figure S2 in the Supporting Information). Decay of this ion occurs with narrowing and intensification of the visible band with a shift in the spectral maximum to ~488 nm, indicative of formation of **{3,4}** (see Figure S2 in the Supporting Information). These spectral changes are essentially the same as previously reported by Raven and Meyer.[27] The decay kinetics exhibited less than first-order

(32) Abragam, A.; Bleaney, B. *Electron Paramagnetic Resonance of Transition Ions*; Dover: New York, 1986.
(33) Lomoth, R.; Magnuson, A.; Xu, Y.; Sun, L. *J. Phys. Chem. A* **2003**, *107*, 4373–4380.
(34) Kasack, V.; W.; Kaim, H.; Binder; Jordanov, J.; Roth, E. *Inorg. Chem.* **1995**, *34*, 1924–1933.
(35) Cotton, F. A.; Torralbe, R. C. *Inorg. Chem.* **1991**, *30*, 2196–2207.

dependence upon the **{4,5}** concentration; plots of log R_o vs log $[\{\mathbf{4,5}\}]_o$, where the subscripts denote initial rates and concentrations, respectively, gave a reaction order $n = 0.84$ at pH 9 in 0.1 M borate buffer over the experimental concentration range of 5−50 μM (see Figure S2 in the Supporting Information). Kinetic complexity was also apparent from the rate profiles obtained at low dimer concentrations, where the decay appeared to be zero-order over most of the reaction course. The initial reaction rate was modestly pH-dependent, increasing ~10-fold over the pH range 2−9,[36] and moderately temperature-dependent, giving phenomenological activation parameters for R_i at 60 μM $[[4,5\}]_o$ of $\Delta H^{\ddagger} = 14$ kcal/mol and $\Delta S^{\ddagger} = -52$ cal/(mol K) over a measured temperature range of 5−55 °C. Quantitative modeling of this reaction was not attempted; its apparent complexity was also noted by Meyer and co-workers.[29]

Raven and Meyer have also reported that **{4,5}** decay was accompanied by stoichiometric formation of O_2 in weakly acidic solutions, but that decay in alkaline media did not generate O_2.[27] We did not observe O_2 formation for this reaction in 100 mM phosphate at either pH 5 or pH 7. Our studies made use of **{4,5}** generated by CPE or by titration with $Ru(bpy)_3^{3+}$ with very sensitive detection afforded by a micro-O_2 electrode immersed directly in the reaction medium. In the electrochemical experiments at pH 7.2, the samples were held at a redox poise of 1.35 V (NHE) for up to 2 h to "burn out" any organic impurities that might be present that would compete effectively with water oxidation.[20,37] Following these experiments, the catalytic activity of the dimers were checked by using them in a well-defined $Ru(bpy)_3^{3+}/S_2O_8^{2-}$ photocatalytic system for O_2 generation;[8] in all cases, rates of O_2 evolution were observed that corresponded to full catalytic activity of the dimer.

As discussed by the Meyer group in their original publication,[3] water oxidation to O_2 would require participation of at least two **{4,5}** ions, implying a complex, multistep process. Direct two-electron oxidation of water to give H_2O_2 as an intermediate product is energetically unfavorable. In acidic media, EPR evidence indicates that **{4,5}** undergoes disproportionation to **{4,4}** and **{5,5}** (discussed below). Given the imposing thermodynamic constraints for water oxidation by **{4,5}**, it seems likely that any O_2 formed in weakly acidic media is due to the presence of **{5,5}** and that decay of **{4,5}** to **{3,4}** in neutral media occurs by preferential oxidative degradation of bipyridine ligands, a reaction that has been demonstrated for monomeric $Ru^{IV}{=}O$[38] and group 8 $M(bpy)_3^{3+}$ complexes in alkaline solutions.[39,40]

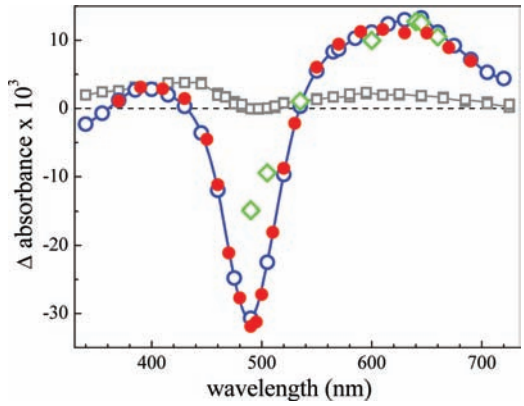

Figure 6. Transient absorption spectrum following pulse radiolysis of **{3,4}**/$S_2O_8^{2-}$/tert-butanol systems. Open symbols, reactions at pH 7.2; solid symbols, reactions at pH 9.2. Squares, prompt absorption change upon completion of reactions 1−3 for Ar-saturated solutions containing 22−25 μM **{3,4}**, 2 mM $S_2O_8^{2-}$, and 5 mM tert-butanol; circles, corresponding changes on microsecond time scale upon completion of reactions 4 and 6 (Figure 7); diamonds, change produced by reaction 4 in N_2O-saturated solutions containing 36 μM **{3,4}** and 0.1 mM $S_2O_8^{2-}$. Red circles, absorption change upon completion of reactions 4 and 6 in Ar-saturated solutions containing 25 μM **{3,4}** and 2 mM $S_2O_8^{2-}$. In all cases, doses generating 0.5 ± 0.05 μM of radicals per unit G value were applied.

Characterization of {4,4}. From the data presented above and in earlier studies, it is evident that **{4,4}** is unstable above pH ~2. To gain information relevant to kinetic analyses, we generated **{4,4}** transiently from **{3,4}** in neutral solutions by using one-electron oxidants ($SO_4^{\bullet-}$, $CO_3^{\bullet-}$) formed by pulse radiolysis.

Reaction with $SO_4^{\bullet-}$. This radical was generated in Ar-saturated solutions containing $K_2S_2O_8$ and tert-butanol. Under these conditions, the major primary radicals from water radiolysis, the hydrated electron and hydroxyl, were scavenged on submicrosecond time scales, as follows

$$S_2O_8^{2-} + e_{aq}^- \rightarrow SO_4^{2-} + SO_4^{\bullet-} \quad (1)$$

$$(CH_3)_3COH + OH^{\bullet} \rightarrow {}^{\bullet}CH_2C(CH_3)_2OH + H_2O \quad (2)$$

where $k_1 = 1.2 \times 10^{10}$ M^{-1} s^{-1} and $k_2 = 6.0 \times 10^8$ M^{-1} s^{-1}.[41] The $SO_4^{\bullet-}$ radical ion that forms is a very strong oxidant ($E^o = 2.43$ V, NHE)[42] that reacts preferentially by electron transfer and was used to oxidize **{3,4}**. The tert-

(36) A similar pH dependence upon decomposition rate was described by Raven and Meyer (see ref 27). Although these researchers originally interpreted their data as first-order in **{4,5}**, subsequent research from the Meyer laboratory revealed a more complex kinetic profile (see ref 29).

(37) In their paper, Raven and Meyer noted that water oxidation by **{4,5}** is extremely sensitive to the presence of organic impurities in the reaction medium, and demonstrated its ability to react with a variety of organic compounds possessing oxidizable functional groups (see ref 27). In principle, our inability to generate O_2 via **{4,5}** decomposition might be attributable to this cause. However, our measured initial rates of **{4,5}** decay are very similar to values that we calculate from their reported kinetic data, suggesting that additional decay channels were not present in our samples. For example, our measured initial rate at pH 7, 23 °C is 14 nM s^{-1}, whereas we calculate a value of ~12 nM s^{-1} from their data at pH 6. While puzzling, this disparity in O_2 evolution results is probably not crucial to understanding water oxidation mechanisms. Both laboratories have presented independent evidence that the catalytically active O_2-evolving state is **{5,5}** (see refs 5, 6, 8, and 29). We have also found that O_2 formation by **{5,5}**-catalyzed reactions is completely quenched in neutral solutions buffered with Tris or citrate, possibly because of displacement of cis-aqua ligands by anation or, more likely, by competitive oxidation of the buffer component by the catalyst. Phosphate and borate buffers could be used over a concentration range of 5−100 mM without any apparent inhibition of activity; we also did not observe any changes in optical, RR, and EPR spectra of the **{3,4}** and **{4,5}** states of the catalyst with concentrations of these salts as high as 250 mM.

(38) Roecker, L.; Kutner, W.; Gilbert, J. A.; Simmons, M.; Murray, R. W.; Meyer, T. J. *Inorg. Chem.* **1985**, *24*, 3784–3791.

(39) Ghosh, P. K.; Brunschwig, B. S.; Chou, M.; Creutz, C.; Sutin, N. *J. Am. Chem. Soc.* **1984**, *106*, 4772–4783.

(40) Hurst, J. K. *Coord. Chem. Rev.* **2005**, *249*, 313–328.

(41) Buxton, G. V.; Greenstock, C. L.; Helman, W. P.; Ross, A. B. *J. Phys. Chem. Ref. Data* **1988**, *17*, 513–886.

(42) Stanbury, D. M. *Adv. Inorg. Chem.* **1989**, *33*, 69–138.

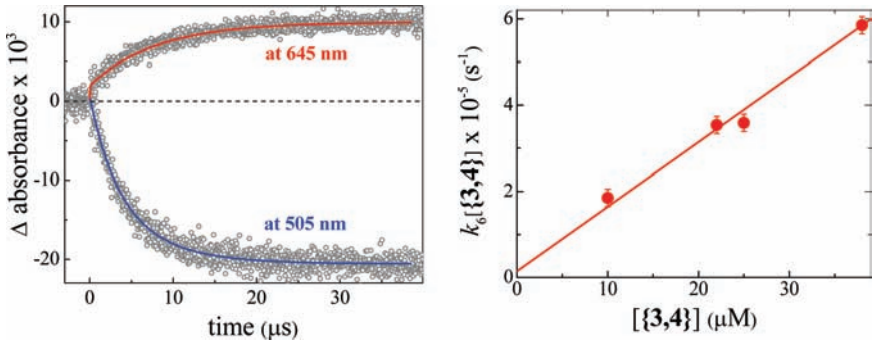

Figure 7. Left: kinetic traces recorded on the microsecond time scale at 645 nm (formation of **{3,3}**, reaction 4) and 505 nm (bleaching of **{3,4}**, reactions 4 and 5) following pulse radiolysis of an Ar-saturated solution containing 22 μM **{3,4}**, 2 mM $S_2O_8^{2-}$, and 5 mM tert-butanol. The small prompt step in the 645 nm trace corresponds to reaction 3. The lines show fits to the data using reactions 4 and 6, resulting in $k_4 = 6.0 \times 10^9$ and $k_6 = 1.6 \times 10^{10}$ M^{-1} s^{-1}. Right: concentration dependence of apparent pseudo-first-order rate constant k_6[**{3,4}**] for **{4,4}** formation via reaction 6; the linear fit slope gives $k_6 = (1.5 \pm 0.2) \times 10^{10}$ M^{-1} s^{-1}.

butanol radical usually decays by self-recombination. In these systems, however, we also observed a spectroscopically distinct species that apparently formed by slow reaction with accumulated **{4,4}**. This reaction is under investigation, and will not be discussed further here other than to note that it did not interfere with the dynamics of formation and spectroscopic characterization of **{4,4}**. The yield of the third primary radical from water radiolysis, the hydrogen atom, is relatively minor, but because it reacts slowly with $S_2O_8^{2-}$ and tert-butanol, it is not scavenged and, as will be shown, rapidly reduces **{3,4}** to **{3,3}**.

Without added **{3,4}**, a transient absorption appeared between 300 and 500 nm during the radiation pulse whose spectrum corresponded closely in both shape and amplitude ($\lambda_{max} = 450$ nm, $\varepsilon_{450} = 1650$ M^{-1} cm^{-1}) to the literature data[43] for the $SO_4^{\bullet-}$ radical (reaction 1). With **{3,4}** present, the immediate transient absorption spectrum (Figure 6, squares) showed characteristic bands of both the $SO_4^{\bullet-}$ radical and **{3,3}** ($\lambda_{max} = 640$ nm, $\varepsilon_{640} = 1.99 \times 10^4$ M^{-1} cm^{-1}). The appearance of the latter can be ascribed to the reaction

$$\{3,4\} + e_{aq}^- \rightarrow \{3,3\} \qquad (3)$$

that occurs in competition with reaction 1. From the initial absorption amplitude at 640 nm, we estimate $k_3 \approx 5 \times 10^{10}$ M^{-1} s^{-1}, that is, about 5% of electrons escape scavenging by $S_2O_8^{2-}$ and participate in reaction 3.

On longer time scales, much larger secondary absorption changes with regions of bleaching and coloration rapidly develop throughout the visible range (Figure 6, circles and diamonds, and Figure 7). The bleaching is due to the consumption of **{3,4}**, which has a strong band centered at 486 nm ($\varepsilon_{486} = 2.56 \times 10^4$ M^{-1} cm^{-1}), and the coloration signals are associated with product formation. Recalling that **{3,3}** has a band around 640 nm, we ascribe the absorption build up there to the reaction

$$\{3,4\} + H^{\bullet} \rightarrow \{3,3\} + H^+ \qquad (4)$$

This reaction was investigated by performing pulse radiolysis in an N_2O-saturated (~25 mM) solution containing only minimal amounts (0.1 mM) of $S_2O_8^{2-}$ (Figure 6, diamonds). Under these conditions, the solvated electrons react nearly quantitatively with N_2O

$$N_2O + e_{aq}^-(+H_2O) \rightarrow N_2 + OH^- + OH^{\bullet} \qquad (5)$$

where $k_5 = 9.1 \times 10^9$ M^{-1} s^{-1},[41] and $SO_4^{\bullet-}$ formation is negligible. Nevertheless, bleaching at ~490 nm and absorption above 600 nm are observed, whose magnitudes are within a few percent of those expected from reaction 4, based on the radiation yield $G(H^{\bullet}) = 0.6$ and the known spectra of **{3,3}** and **{3,4}**. From the absorption kinetics, the rate constant $k_4 = (6 \pm 1) \times 10^9$ M^{-1} s^{-1} was derived.

The bleaching half-time of the 486 nm band (Figure 7) is nearly two times shorter than the coloration half-time at greater than 600 nm. Moreover, the difference spectrum observed at the end of these processes (Figure 6, circles) did not quantitatively correspond to reaction 4; the extent of bleaching was much greater than expected for just this reaction. These facts indicate the occurrence of another reaction, which must be the one-electron oxidation of **{3,4}**

$$\{3,4\} + SO_4^{\bullet-} \rightarrow \{4,4\} + SO_4^{2-} \qquad (6)$$

From the measured transient spectrum in Figure 6, known spectra of **{3,3}** and **{3,4}**, and the known radiation yields for $H^{\bullet}$ and $SO_4^{\bullet-}$, we obtain the absorption spectrum of **{4,4}** shown in Figure 8. This spectrum displays a symmetrical band centered at 487 nm with $\varepsilon_{487} = 1.8 \times 10^4$ M^{-1} cm^{-1}.

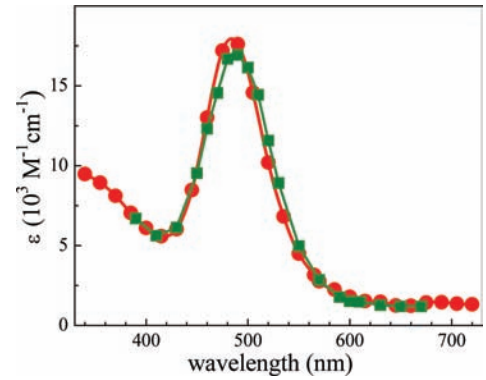

Figure 8. Absorption spectra of **{4,4}** at pH 7.2 obtained in the persulfate system (red circles) and at pH 10.5 in the carbonate system (green squares).

(43) Huie, R. E.; Sieck, L. W. SOx Radical Monoanions−Reactions in Solution and in the Gas Phase. In *S-Centered Radicals*; Alfassi, Z. B., Ed.; Wiley: Chichester, U.K., 1999; pp 63−95.

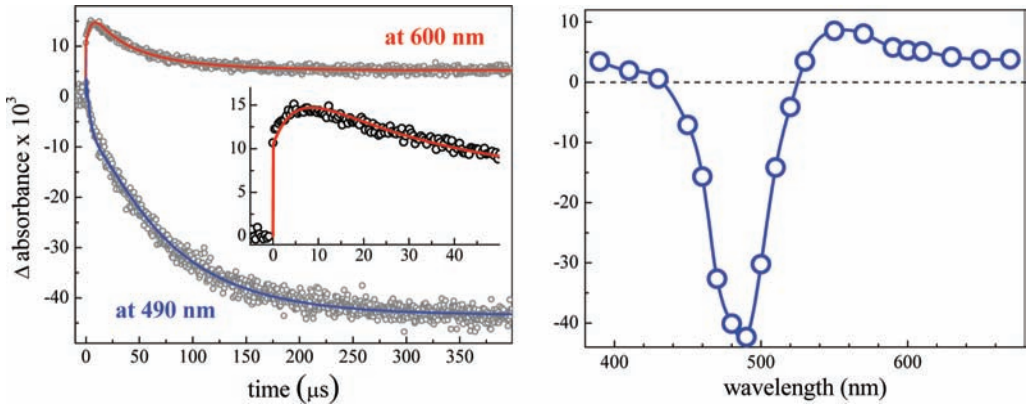

Figure 9. Left: kinetic traces recorded at 490 and 600 nm following pulse radiolysis of an N_2O-saturated solution containing 38 μM **{3,4}**, 30 mM carbonate, pH 10.5, and 0.1 mM $S_2O_8^{2-}$; the inset shows the initial part of the 600 nm kinetic trace. The lines are fits to the data obtained by numerical simulation (see text for details). Right: transient absorption spectrum at 400 μs.

The same transient spectrum was obtained when measurements were made in borate buffer at pH 9.2 (Figure 6, solid circles); moreover, the derived spectrum is identical within experimental uncertainty to that of **{4,4}** prepared by CPE in 0.5 M triflic acid, for which $\lambda_{max} = 488$ nm and $\varepsilon_{488} = 1.6 \times 10^4$ M^{-1} cm^{-1}.[17]

Because the spectra of all species involved in reactions 4 and 6 are now known, the rate constant for reaction 6 can be determined by modeling the bleaching kinetics at 505 nm at various concentrations of **{3,4}** with k_6 as the only adjustable parameter. This analysis yields the k_6[**{3,4}**] vs [**{3,4}**] dependence shown in Figure 7, from which $k_6 = (1.5 \pm 0.2) \times 10^{10}$ M^{-1} s^{-1} at 11 mM ionic strength. The small intercept in this plot corresponds to self-decay of $SO_4^{\bullet-}$. The concentration ratio of **{3,3}** to **{4,4}** produced in reactions 4 and 6, respectively, is about 0.2. Notably, the k_3, k_4, and k_5 values are close to those reported for analogous reaction of e_{aq}^-, H$^\bullet$, and $SO_4^{\bullet-}$ with other Ru-bipyridyl complexes; in all cases, these reactions are essentially diffusion-controlled.[44−48]

Reaction with $CO_3^{\bullet-}$. The oxidation of **{3,4}** by the $CO_3^{\bullet-}$ radical ($\lambda_{max} = 600$ nm, $\varepsilon_{max} \approx 1950$ M^{-1} cm^{-1}, $E^o = 1.55-1.59$ V, NHE)[49−51]

$$\{3,4\} + CO_3^{\bullet-} \rightarrow \{4,4\} + CO_3^{2-} \qquad (7)$$

was investigated at pH 10.5 in an N_2O-saturated, 30 mM carbonate solution where the hydrated electrons are converted into OH$^\bullet$ (reaction 5); the latter is used to generate $CO_3^{\bullet-}$ by reaction primarily with dibasic carbonate

$$CO_3^{2-} + OH^\bullet \rightarrow CO_3^{\bullet-} + OH^- \qquad (8)$$

where $k_8 = 3.9 \times 10^8$ M^{-1} s^{-1}.[41] Under our experimental conditions, $CO_3^{\bullet-}$ formation was complete within 0.5 μs.

The kinetics and transient spectra obtained in this system are shown in Figure 9. The two most obvious differences between these and the data in Figures 6 and 7 are the much slower rate of absorption changes and the absence of an absorption band around 640 nm in the microsecond transient spectrum. The former observation indicates that reaction 6 is substantially more rapid than reaction 7, and the latter that **{3,3}** does not accumulate as a long-lived transient despite the presence of reaction 4 as a major pathway for H$^\bullet$ decay. However, transient absorption is observed above 600 nm on shorter time scales (Figure 9), the intensity of which peaks at ~10 μs, then decays to baseline values. These cumulative data can be quantitatively reconciled by introducing a rapid reaction

$$\{3,3\} + CO_3^{\bullet-} \rightarrow \{3,4\} + CO_3^{2-} \qquad (9)$$

in which **{3,3}** produced by reaction 4 is reoxidized to **{3,4}**, thus eliminating the **{3,3}** absorption in the product spectrum (Figure 9) and reducing the overall yield of **{4,4}**. Reactions 4 and 9 also generate the 600 nm maximum in the kinetic profiles, which monitors formation and decay of **{3,3}**.

Numerical simulation of the kinetics using a mechanism consisting of reactions 4, 7, 9, and the $CO_3^{\bullet-} + CO_3^{\bullet-}$ self-recombination ($k = 2 \times 10^7$ M^{-1} s^{-1})[51] gave good fits over the entire spectral range with $k_7 = 4 \times 10^8$ and $k_9 \approx 2 \times 10^{10}$ M^{-1} s^{-1} (Figure 9). Thus $CO_3^{\bullet-}$ oxidizes **{3,4}** almost 40 times slower than does $SO_4^{\bullet-}$, which may be the consequence of the ~20 kcal/mol less-favorable energetics of reaction 7 compared to reaction 6. The large difference in rates of these reactions account for the accumulation of **{3,3}** in the persulfate system. Specifically, in that case, radiolytically generated $SO_4^{\bullet-}$ is rapidly consumed by reaction with excess **{3,4}**, so that little is available for reoxidation of **{3,3}**, which is rapidly formed in reactions 3 and 4; in contrast, sufficient $CO_3^{\bullet-}$ persists during formation of **{3,3}** to reoxidize it to **{3,4}**. Because reaction 9 is already close to the diffusion limit with $CO_3^{\bullet-}$, it will not be

(44) Baxendale, J. H.; Fiti, M. *J. Chem. Soc., Dalton Trans.* **1972**, 1995–1998.
(45) Meisel, D.; Matheson, M. S.; Mulac, W. A.; Rabani, J. *J. Phys. Chem.* **1977**, *81*, 1449–1455.
(46) Jonah, C. D.; Matheson, M. S.; Meisel, D. *J. Am. Chem. Soc.* **1978**, *100*, 1449–1456.
(47) Mulazzani, Q. G.; Dangelantonio, M.; Camaioni, N.; Venturi, M. *J. Chem. Soc., Faraday Trans.* **1991**, *87*, 2179–2185.
(48) Gorner, H.; Stradowski, C.; Schulte-Frohlinde, D. *Photochem. Photobiol.* **1988**, *47*, 15–29.
(49) Huie, R. E.; Clifton, C. L.; Neta, P. *Radiat. Phys. Chem.* **1991**, *38*, 477–481.
(50) Czapski, G.; Lymar, S. V.; Schwarz, H. A. *J. Phys. Chem. A* **1999**, *103*, 3447–3450.
(51) Lymar, S. V.; Schwarz, H. A.; Czapski, G. *Radiat. Phys. Chem.* **2000**, *59*, 387–392.

significantly faster with $SO_4^{\bullet-}$. Thus, the sulfate radical will react preferentially with **{3,4}**.

The simulations also provide an apparent radiation yield of 4.5 for **{4,4}** in the carbonate system. With this value, the transient absorption in Figure 9 was converted into the spectrum of **{4,4}** plotted in Figure 8, which is identical within experimental uncertainty to the spectrum at pH 7.2, and as noted above, for the directly determined spectrum at pH 0.3.[17] Thus, either the extent of protonation of coordinated aqua ligands is invariant over this range, that is, there is no pK_a for **{4,4}** between pH 0.3−10, or the optical spectra of the various protonation states are indistinguishable. By analogy with the properties of the corresponding Os dimer (discussed below), we infer that the molecular formula of **{4,4}** is $[Ru(bpy)_2(OH)]_2O^{4+}$ below pH 10.

The **{4,4}** complex obtained by reactions 6 and 7 is unstable in neutral solution and undergoes further reaction(s) on the time scale of milliseconds to minutes leading to regeneration of **{3,4}**. These processes are being investigated.

Accumulation of **{4,4}** in Acidic (pH <2) Solutions. Although both **{4,4}** and **{4,5}** are unstable in acidic media, there are conditions under which one of these intermediates accumulates. For example, in rapid CPE titrimetric studies, we have been able to acquire its RR spectrum, and decomposition of electrochemically prepared **{5,5}** to **{3,4}** is markedly biphasic, proceeding through the same intermediary species.[17] The identity of this intermediate is not generally agreed upon. On the basis of primarily redox titrimetric results and their interpretation of multimixing kinetic experiments, Meyer and co-workers have assigned it an oxidation state of **{4,5}**,[3,29,52] whereas our redox titrimetric and physical characterization studies are consistent only with an oxidation state of **{4,4}**. The data supporting our assignment as **{4,4}** have been summarized;[6] two additional observations emanating from the present study that bear upon this issue are described below. First, the electrochemical behavior of the osmium analog of the "blue dimer", $[Os(bpy)_2(OH_2)]_2O^{4+}$, has been interpreted in terms of the following oxidation sequence: **{3,3}** → **{3,4}** → **{4,4}** → **{5.5}**, i.e., with **{4,4}** accumulating as a stable intermediate.[18] The pH dependence of redox potentials indicates that the cis-oxo ligands should be protonated in this oxidation state, i.e., that the structure is $[Os^{IV}(bpy)_2(OH)]_2O^{4+}$. Consistent with this interpretation, we find no vibrational band attributable to an Os=O stretching mode in the RR spectrum of **{4,4}** in 0.5 M triflic acid, unlike the strong band associated with **{4,5}** in neutral media (see Figure S1 in the Supporting Information). The RR spectra of the "blue dimer" parallel those of the Os analog; specifically, no Ru=O mode was detected in the intermediate accumulating in acid solution,[17] whereas this band is a dominant feature of **{4,5}** in neutral solutions (Figure 4B). Second, EPR spectra taken of CPE-generated **{4,5}** solutions immediately following a pH jump from 7.2 to 0.3 showed complete disappearance of its characteristic broad rhombic signal, accompanied by formation of a sharper axial $g = 2.01$ signal that has been

(52) Chronister, C. W.; Binstead, R. A.; Ni, J.; Meyer, T. J. *Inorg. Chem.* **1997**, *36*, 3814–3815.

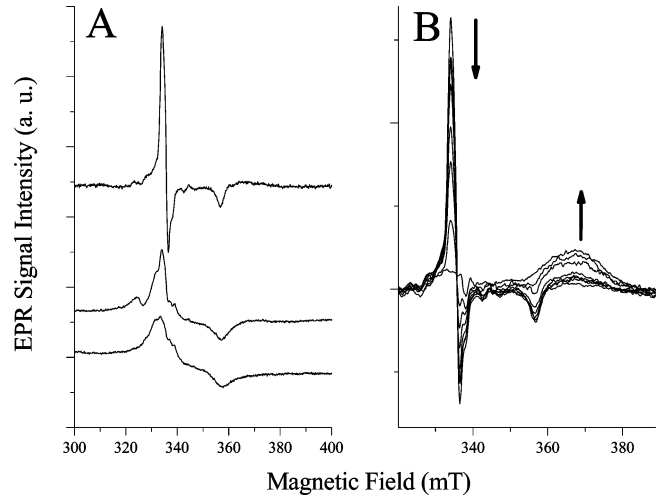

Figure 10. CW-EPR-detected disproportionation of **{4,5}** below pH ~2. (A) CPE-generated **{4,5}** in 10 mM phosphate, pH 7.2, that was subsequently pH-jumped to pH 0.3 by rapid 1:1 mixing with 1 M triflic acid (upper trace); CPE-prepared **{4,5}** in 100 mM phosphate, pH 3.5 (middle trace); CPE-prepared **{4,5}** in 100 mM phosphate, pH 7.2 (lower trace). (B) Slow decay of the initially observed signal following the pH jump to that of the final product (**{3,4}**); spectra were recorded over the range of 0−2100 s. Instrument parameters: ~9.484 GHz microwave frequency, 100 kHz modulation frequency, 15 gauss modulation amplitude, 20 ms conversion time, 10 ms time constant, 20 mW microwave power.

associated with oxidation to the **{5,5}** level.[17,31,53] An EPR spectrum of the immediate product is shown in Figure 10A (upper trace). The **{3,4}** ion could not be detected in the initial spectrum, although it slowly accumulated with time, as shown in Figure 10B. For comparative purposes, the spectra of CPE-prepared **{4,5}** at pH 3.5 and 7.2 are also shown (middle and lower traces, respectively); the former spectrum is notable in exhibiting the simultaneous presence of **{4,5}**- and **{5,5}**-associated axial signals. The changes in EPR spectra following the pH jump (Figure 10B) can be interpreted as indicating rapid disproportionation of **{4,5}** in acidic media to **{5,5}** and the EPR-silent **{4,4}**, i.e., the reaction 2**{4,5}** → **{4,4}** + **{5,5}**, with slower subsequent oxidation of water by **{5,5}**, resulting ultimately in complete conversion to **{3,4}**. Thus, from these experiments as well, we infer that **{4,4}** is the intermediate accumulating in strongly acidic solutions.

Concluding Comments

The cumulative data support the following reaction scheme for water oxidation catalyzed by the "blue dimer" (see Scheme 1).

At first glance, the redox properties of the "blue dimer" may appear unusual in that **{4,5}** is thermodynamically unstable at low pH, whereas **{4,4}** is unstable under more alkaline conditions. However, this behavior is shared by the Os analog, for which Meyer and co-workers have provided a cogent rationalization in terms of the influence of protic

(53) Like **{4,4}**, **{5,5}** is zero- or even-spin and therefore should be EPR-silent in the X-band spectrum. On the basis of its physical properties, including symmetry, hyperfine coupling, and saturation characteristics, we have suggested that this signal is due to a ligand-centered radical cation formed by internal electron transfer in **{5,5}**, e.g., $[Ru^{IV}(bpy)(bpy^{\bullet+})(OH)-O-Ru^{V}(bpy)_2(O)]^{4+}$ (see refs 6 and 8).

Scheme 1. Thermodynamically Accessible Redox States of the "Blue Dimer"

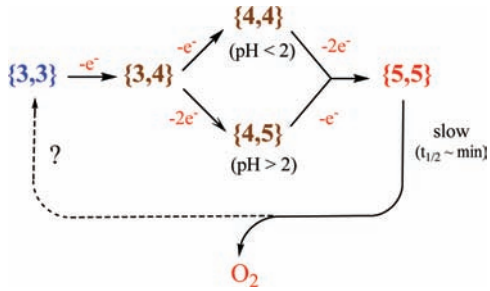

equilibria upon reduction potentials for the individual half-reactions.[18] This group has also reported that **{4,5}** is unstable at pH $\leq$ 2 in the structurally similar $[Ru(tpy)(OH_2)_2]_2O^{4+}$ ion, although in this case **{4,4}** was stable over the entire accessible pH range.[54] In any event, our assignments have precedents in the redox properties of other group 8 μ-oxo ions. The one-electron reduction potentials for **{5,5}**, **{4,5}**, and **{4,4}** nearly converge in strongly acid solutions, so that it is possible that medium effects could alter their relative stabilities. These conditions necessarily impose high anion concentrations, which can introduce complications such as precipitation of higher oxidation states, as has been demonstrated for ClO_4^-,[27,30,52] or catalyst inactivation by anation at the water coordination sites during either catalytic turnover[29,54] or complex preparation,[7,20] that can dramatically affect the outcome of experimental measurements. The conditions used in our studies were chosen to minimize these types of interferences.

(54) Lebeau, E.; Adeyemi, S. A.; Meyer, T. J. *Inorg. Chem.* **1998**, *37*, 6476–6484.

Acknowledgment. The authors thank Professor Jeanne McHale of the Washington State University Chemistry Department for making available her Raman facility for these studies, Jon Downing for technical assistance in acquiring the RR spectra, Professor David Kramer for use of the WSU EPR Center, and Dr. Harold Schwarz of the Brookhaven National Laboratory Chemistry Department for adapting the pulse radiolysis data analysis programs to our needs. The research done at WSU was supported financially by the Chemical Sciences, Geosciences and Biosciences Division, Office of Basic Energy Sciences, Office of Science, U.S. Department of Energy, under Grant DE-FG02-06ER15820; research at BNL was carried out under the auspices of the U.S. Department of Energy under contract DE-AC02-98CH10886 from the Division of Chemical Sciences, Office of Basic Energy Sciences.

Supporting Information Available: Resonance Raman spectra of the redox states of the $[Os(bpy)_2(OH_2)]_2O^{4+}$ ion (Figure S1) and the decay kinetics of **{4,5}** absorption at pH 7.2 (Figure S2), with accompanying textual description (PDF). This material is available free of charge via the Internet at http://pubs.acs.org.

IC9001219